MORTARLESS REINFORCED CONCRETE MASONRY WALL UNDER CONCENTRATED AXIAL LOAD AND TRANSVERSE LOAD

Sittichai Seangatith[1]

ABSTRACT: This paper presents the results of a study of the short-term behavior of mortarless reinforced concrete masonry wall subjected to two types of loading: concentrated axial load and transverse load. The specimens were made of standard hollow concrete masonry unit, reinforcing steel bar, and grout. The variables studied were steel reinforcement ratio, height or span of the specimen, and grouting pattern. A total of 40 specimens were tested, including 24 specimens under concentrated axial load and 16 specimens under transverse load. The experimentally obtained results were correlated to the ACI 530-99 design equations for reinforced mortar jointed wall and statistical analyses were performed. Finally, the design equations were adjusted based on the obtained results.

Key Words: Mortarless masonry, Masonry wall, Concrete masonry unit

1. INTRODUCTION

The mortarless masonry or dry-stacked masonry differs from traditional masonry in that no mortar is used in the construction. Historical evidence at fort Porta Nigra, Tier, Germany, shows that this concept was originated about 1800 years ago [1]. Recently, this concept has been used in many countries such as Germany and USA due to the development in masonry unit production leading to well leveled units with small tolerances of size and shape. Typically, the units used in mortarless masonry are the same as those used in masonry with thin mortar layer. Sometimes, they are in the form of interlocked masonry units to ensure the interlocking between them. The units can be both solid and hollow masonry unit. Solid block units are popular in Europe, while hollow concrete block units which are stacked and grouted with or without reinforcement afterward are popular in USA [2]. Construction with mortarless masonry is an attractive alternative to conventional masonry with mortar joint due to the construction efficiency and economy. It eliminates the uses of mortar in head joint and bed joint, reducing the material and labor cost as well as cutting the mortar curing time. It also requires less skilled labor and the masonry units can be laid easier and quicker, offering labor cost and time savings.

Marzahn [2, 3] performed experimental investigation on structural behavior of dry-stacked masonry and mortar-jointed masonry walls subjected to uniform compression perpendicular to the bed plane. The experimental setup consisted of masonry specimens with five units high and two units wide, according to German standard DIN 18554, and five units high and one unit wide. The specimens were made of solid calcium silicate units and autoclaved aerated concrete units. The surfaces of the units were machined to create different bedding conditions. A thin mortar layer was used to build the mortar-jointed masonry specimens. In comparison with mortar-jointed masonry wall, initial deformation of the dry-stacked masonry wall had a larger volume of the plastic parts, indicating that the masonry units have to settle down in

[1] *Asst. Prof., Suranaree University of Technology, Thailand, sitichai@ccs.sut.ac.th*

order to balance uneven surface before they can carry loads. This initial deformation was observed up to about 30% of the compressive strength of the wall. The compressive strength of the dry-stacked masonry wall was up to 85-95% of that of the mortar jointed masonry wall. This lower strength is mainly due to the quality of the unit such as differences in height and uneven bed surface between each unit. The dry-stacked masonry wall failed differently from the mortar jointed masonry wall. It failed similar to concrete and the collapse occurred by formation of shearing line in diagonal direction, while the mortar jointed masonry failed in the form of wall splitting in the plane of the wall. It was also concluded that the bedding conditions have small effect in decreasing the compressive strength of the dry-stacked masonry walls.

In developing countries, the demands for low-cost buildings such as houses, farm buildings, and small industrial buildings, are in great number. These buildings should be high-quality permanent structures so that maintenance is minimum and are should be produced in shorter time to catch up with the increasing needs. Recently, the uses of the load-bearing concrete masonry wall are increasingly popular due to its low-cost and easy-to-build into any shapes. In addition, due to the advantages of the mortarless masonry as previously mentioned, the concept of mortarless reinforced concrete masonry wall built by using typical concrete masonry unit has been proposed and studied. This paper present the results of a study on the short-term behavior of the masonry wall subjected to concentrated axial load and transverse load.

2. MECHANICAL PROPERTIES OF THE COMPONENT AND MASONRY

All masonry walls were constructed using standard hollow load-bearing concrete masonry units laid in running bond, grouted by coarse grout, and reinforced by steel reinforcing bars. The concrete unit had the actual dimensions of 390 mm long by 190 mm high and 140 mm thick with the dimension tolerances of less than ± 3 mm as specified in ASTM C90. The grout had mix proportion as specified in ASTM C476 (Type I Portland cement: fine aggregate: coarse aggregate of 1: 2.25: 2 by volume) and slump in the range of 250 and 280 mm. Samples of the masonry unit and grout were taken and tested at regular interval throughout this testing program. Two types of mortarless prism, partially grouted and fully grouted, were also built and tested to determine the compressive strength and modulus of elasticity of the mortarless masonry. Table 1 presents the summary of the geometric and mechanical properties of the concrete masonry unit, grout, and prism. Steel reinforcing bars were the same as used in reinforced concrete work specified in ASTM 615. Table 2 shows the yielding stresses and allowable stresses of the reinforcing bars.

In order to compare the behavior and the compressive strength of the mortarless and mortar-jointed masonry prisms, two types of mortar-jointed prisms, partially grouted and fully grouted, were also built using type N mortar (1: 3 cement: sand by volume) with 120 percent flow and tested as specified in ASTM C270. Type N mortar was used to provide a lower bound to the results. The test results are shown in Table 1. In comparison, the partially grouted and fully grouted mortarless prisms had the compressive strength of 85% and 92% of those of the partially grouted and fully grouted mortar-jointed prisms, respectively. The mortarless prisms had a larger initial deformation in the first load level, up to 35% of the compressive strength, comparing to about 15% of that of the mortar-jointed prisms as shown in Fig. 1. These results are similar to those reported by Marzahn [1]. By preloading the prism

specimens to 30% of their compressive strength, it was observed that the initial deformations were reduced significantly upon reloading. The failure mode of these two types of prisms, however, were similar in the form of wall splitting in their own plane as shown in Fig. 2.

Table 1 Geometric and mechanical properties of concrete unit, grout, and prism

	Dimensions (*l*)(*h*)(*t*) (mm)(mm)(mm)	Test Method	No. of specimens	Compressive strength		Modulus of elasticity (GPa)
				Mean (MPa)	COV (%)	
Concrete unit	(390)(190)(140)	ASTM C140	24	9.62	8.1	-
Grout	190 mm cube	ASTM C1019	24	16.51	10.6	-
Partially grouted mortarless prism	(390)(570)(140)	ASTM E447	9	8.58	11.9	4.88
Fully grouted mortarless prism	(390)(570)(140)	ASTM E447	9	12.98	11.4	5.42
Partially grouted prism	(390)(590)(140)	ASTM E447	9	9.80	11.7	-
Fully grouted prism	(390)(590)(140)	ASTM E447	9	14.03	11.7	-

Note: (1) The compressive strengths were calculated using net cross-sectional area of 27,900 mm^2 for concrete units, 41,250 mm^2 for partially grouted prisms, and 54,600 mm^2 for fully grouted prisms.

(2) Partially grouted prism is the prism having one hollow cell grouted and the fully grouted prism is the prism having both two hollow cells grouted.

Table 2 Yielding stress and allowable stresses of reinforcing bars

Type	Test Method	Yielding stress (MPa)	Allowable compressive stress (MPa)	Allowable tensile stress (MPa)
RB9	ASTM E8	328.3	131	140
DB12	ASTM E8	356.4	142	140
DB16	ASTM E8	445.9	165	165

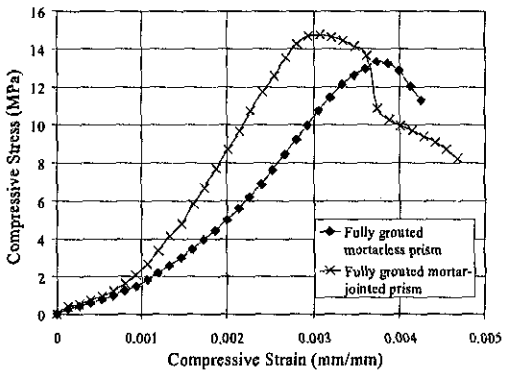

Fig. 1 Compressive stress-strain curves of masonry prisms

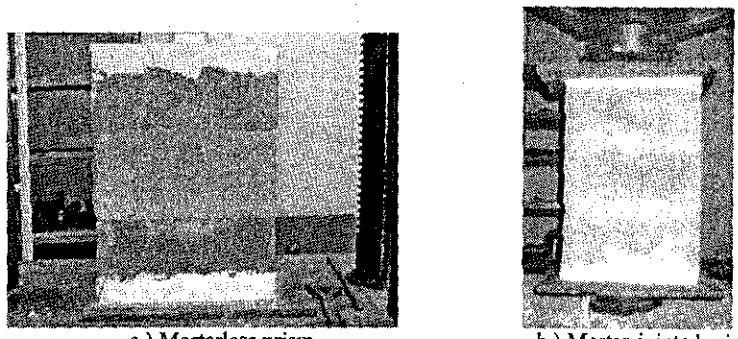

a.) Mortarless prism. b.) Mortar-jointed prism.

Fig. 2 Typical cracks in masonry prisms

Since there is no building code for the design of mortarless reinforced concrete masonry walls, the walls specimens used in this study were preliminarily designed and detailed in accordance with ACI 530-99. Table 3 and 4 show the details of the specimens for the concentrated axial load test and the transverse load test, respectively. They had three-unit wide by four-, thirteen-, and fifteen-course high, which were considered large enough to be representative of the walls. In each type of the tests, the specimens were constructed in four groups having the cross-sections as shown in Fig. 3.

Table 3 Details of test specimen for concentrated axial load test

Specimen number	Reinforcing bars for 1 grouted cell	Reinforcement ratio, ρ (%)	Height, h (m)	Slenderness ratio, h/r	Grouting pattern	No. of specimen
C1-076-P	2-DB12	0.55	0.760	17.3	Partial	2
C1-247-P	2-DB12	0.55	2.470	56.4	Partial	2
C1-285-P	2-DB12	0.55	2.850	65.0	Partial	2
C2-076-P	2-RB9	0.47	0.760	18.8	Full	2
C2-247-P	2-RB9	0.47	2.470	61.1	Full	2
C2-285-P	2-RB9	0.47	2.850	70.5	Full	2
C3-076-P	2-DB16	0.97	0.760	17.3	Partial	2
C3-247-P	2-DB16	0.97	2.470	56.4	Partial	2
C3-285-P	2-DB16	0.97	2.850	65.0	Partial	2
C4-076-P	2-DB12	0.83	0.760	18.8	Full	2
C4-247-P	2-DB12	0.83	2.470	61.1	Full	2
C4-285-P	2-DB12	0.83	2.850	70.5	Full	2

Table 4 Details of test specimen for transverse load test.

Specimen number	Reinforcing bars for 1 grouted cell	Reinforcement ratio, ρ (%)	Span length, L (m)	Grouting pattern	No. of specimen
F1-237-P	2-DB12	0.27	2.37	Partial	2
F1-275-P	2-DB12	0.27	2.75	Partial	2
F2-237-P	2-RB9	0.23	2.37	Full	2
F2-275-P	2-RB9	0.23	2.75	Full	2
F3-237-P	2-DB16	0.48	2.37	Partial	2
F3-275-P	2-DB16	0.48	2.75	Partial	2
F4-237-P	2-DB12	0.41	2.37	Full	2
F4-275-P	2-DB12	0.41	2.75	Full	2

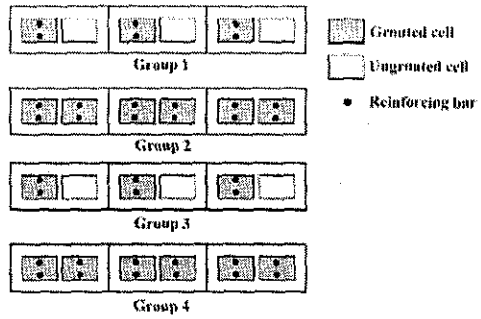

Fig. 3 Cross-sections of the wall specimens

All specimens were built in the laboratory by an experienced mason using normal construction procedures and were air-cured for at least 28 days before testing. Two specimens were tested for each specimen number. The specimen identification number has the following meanings: the first letter and number indicates type of testing (C for concentrated axial load test, F for transverse load test) and specimen group, the second number indicates specimen height or span, and the last letter indicates grouting pattern (P for partial grouting, F for fully grouting). For example, C1-076-P is the specimen for concentrated axial load test, group 1, 0.760 m high, and partially grouted. It should be noted that, for the concentrated axial load test, the reinforcement ratio, ρ, is the ratio of the total reinforcing bar area in one masonry unit to the net cross-sectional area of the masonry with one unit wide. For the transverse load test, the reinforcement ratio is half of the value for the concentrated axial load test because only the tensile reinforcing bars were considered to effectively resist the applied load. The slenderness ratio is the height of the specimen, h, divided by the minimum radius of gyration, r, of its cross-section.

3. TEST SET-UP

Fig. 4 shows the test set-up for the concentrated axial load test and for the transverse load test. The loading frame was used to apply the loads to the specimens. For the concentrated load test, the axial load was applied through steel bearing plate of 200 mm wide, 150 mm long, and 25 mm thick. This gives a bearing load-area ratio (the ratio of the area of the bearing plate to the total cross-sectional area of the specimens) of 12.8%. The bearing plate was set lengthwise on a plaster bed on the top of the specimens at one of the grouted cell near the centerline of the specimen. The bottom end was set directly on a thin layer of plaster on the reaction floor. The axial deformation at the loading point and the lateral deflection at the mid-height were monitored by two dial gages at each location. For the transverse load test, the specimens were supported by two rigid steel beams, having the same length as the specimen width, at both ends. Due to support configuration, the spans of the specimens equal to the overall length subtracted by 0.010 m. The specimens were subjected to the four-point loading at one-third point of the span. The lateral deflection at the mid-span was measured by three dial gages; one at the center and one at each of the two edges. According to the test results obtained in the prism test, a preload of 30% of the estimated ultimate loads was applied before the beginning of the test to settle down the uneven bed surfaces of the masonry units and then unloaded to about 2 kN to seat the specimen into the testing position. All specimens were tested until they failed.

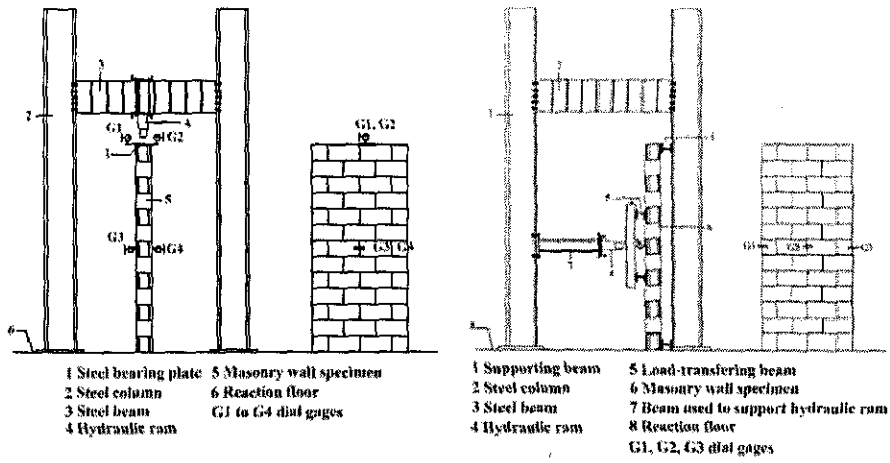

a.) Concentrated axial load test. b.) Transverse load test.

Fig. 4 Test set-up for mortarless masonry wall tests

4. RESULTS AND DISCUSSIONS

4.1 Behavior and Mode of Failure of the Specimens under Concentrated Axial Load

During the preloading, it was observed that cracks developed randomly in the test specimens due to the uneven surfaces of the masonry units, similar to that observed in the prism tests. These cracks can be classified into two types. The first type is due to load transfer caused by unequal friction that obstructs lateral deformation of the masonry units. These cracks were developed along the edges of the head joints and extended through the masonry units above and below as shown in Fig. 5.a. The second type is due to flexural movements caused by height tolerances of the masonry units in a course. These cracks were developed along the edges of the head joints and extended through the masonry units below as shown in Fig. 5.b. These flexural cracks were usually accelerated when a higher load was applied until there is full contact between the masonry units.

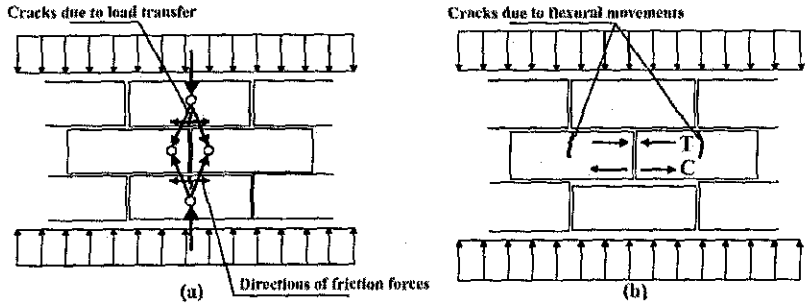

Fig. 5 Cracks due to the uneven bed surfaces of the units

Fig. 6 shows a typical plot of the axial load-axial deformation for the concentrated axial load test. The specimens showed a linear response up to 65-80% of the ultimate axial load. Increasing the applied load within this linear range, the cracks observed during preloading continued to increase in size, but did not influence the response of the specimens. As the load approached the linear limit, vertical cracks occurred on the face shell directly in line with the

edges of the bearing plate. These cracks were formed by the bearing plate tearing against the masonry. Further increase the applied load beyond the linear limit, the slope of the curve decreased until the applied load reached the ultimate load. Finally, the applied load dropped with significant increase in the axial deformation. Generally, specimens failed by tearing and crushing of the masonry in the region beneath the bearing plate with shear line in the diagonal direction. The shear line extended from the bearing plate along the specimen height at the angle of 20 to 30 degree to the vertical for fully grouted specimens and at the angle of 25 to 35 degree for partially grouted specimens as shown in Fig. 7. Differences in the shear line angles indicate that the grout and reinforcing bars can reduce the magnitude of load dispersion angle under the bearing plate. It should be noted that these angles are more severe than the frequently assumed value of 45 degree typically used in design since the masonry area supporting the applied load was reduced by nearly 50% [12].

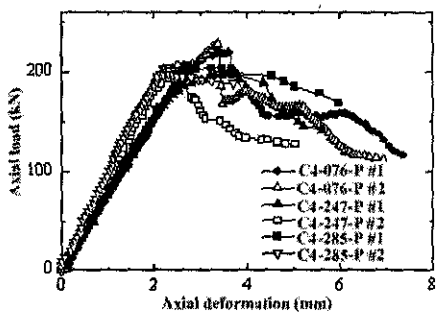

Fig. 6 Typical axial load-axial deformation curves for concentrated axial load test

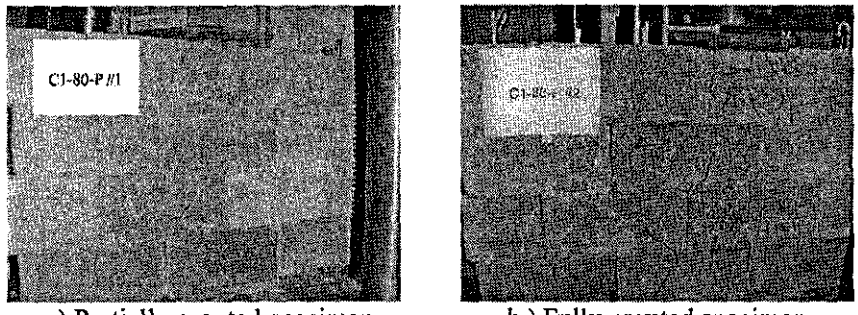

a.) Partially grouted specimen b.) Fully grouted specimen

Fig. 7 Cracks in the test specimens due to concentrated axial loads

Fig. 8 shows a typical plot of the ultimate concentrated axial load versus slenderness ratio. Increasing the slenderness ratio decreased the ultimate axial loads slightly. Since all specimens failed in the same mode as described in the previous paragraph, the decrease in the ultimate axial load must have been due to unavoidable factors such as misalignment of the specimen, specimen's out-of-straightness, and eccentricity of the applied load. It was also found that increasing the reinforcement ratio and grouting area did not increase the ultimate loads. This insensitivity of the ultimate loads is due to the fact that all specimens have equal load-bearing area and the reinforcing bars yielded at the strain well below the ultimate strain of the masonry. In addition, by examining the cracks in the region under the bearing plate, it was found that no crack extended passing the head joint to the adjacent masonry units in the

same course. This indicates that there was no stress transfer through the head joint. Therefore, the plate bearing area should be used to calculate the ultimate stress of the wall specimens.

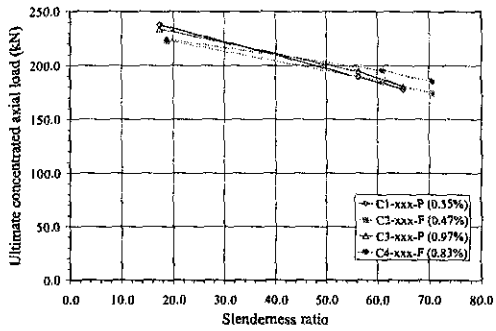

Fig. 8 Ultimate concentrated axial load versus slenderness ratio

4.2 Behavior and Mode of Failure of the Specimens under Transverse Load

Fig. 9 shows the typical curves of the applied transverse load versus lateral deflection at mid-span. Generally, the curves consist of two linear segments, indicating that the specimens had a bilinear behavior with a larger stiffness in the first linear segment. Following the flexural analysis for the reinforced masonry wall presented in [13], it was found that the tensile steel reinforcing bars yielded near the end of the first linear segment, thus reducing the stiffness of the second linear segment. Therefore, the bending moment that the transverse load causes the yielding of the tensile steel reinforcing bars or yielded transverse load was taken as the flexural strength of the masonry specimen. At the end of the tests, the maximum transverse loads were in the range of 10 to 25% greater than that of the yielded transverse load. All specimens failed by large tensile cracks along the bed surfaces of the masonry units on the tension zone of the specimens and crushing of the masonry units on the compression surface as shown in Fig. 10.

Fig. 11 shows the plot of the flexural strength versus steel reinforcement ratio for different span lengths and grouting patterns. The flexural strength at zero reinforcement ratio was calculated using modulus of rupture of the grout and the classical flexural formula. The modulus of rupture was determined by using 9 grout specimens according to ASTM C78 and was found to be 2.024 MPa. Using linear regression analysis, it can be seen that the relationship between the flexural strength and the steel reinforcement ratio is linear, which is in good agreement with the flexural theory in [13]. As expected, increasing the steel reinforcement ratio and the grouting area increase the flexural strength, but increasing the span length decreases the flexural strength.

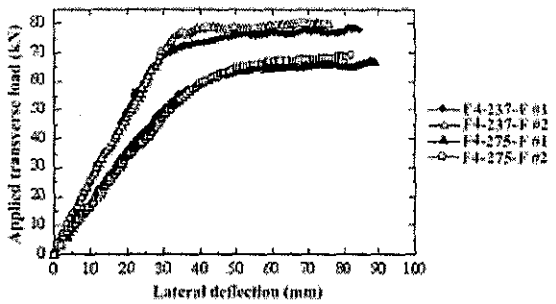

Fig. 9 Typical applied transverse load versus lateral deflection

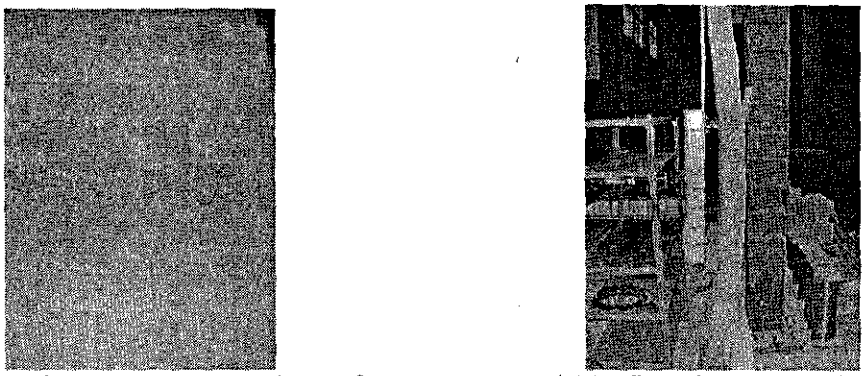

a.) Crushing lines on the compression surface b.) Deflected shape at failure

Fig. 10 Typical mode of failure of the specimens due to transverse loads

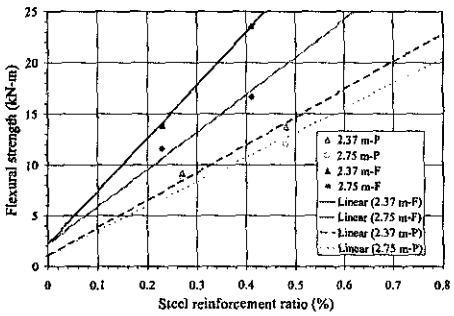

Fig. 11 Flexural strength versus steel reinforcement ratio

4.3 Comparisons of the Concentrated Axial Load Test Results with the Design Equations

Table 5 shows the observed ultimate axial load, P_{ult}, along with the allowable axial load, P_a, the proposed allowable axial load, P_a', and the ratios of the ultimate axial load to the allowable load. Since the slenderness ratios of the wall specimens used in this study were less than 99, the ACI allowable axial load was calculated by using the equation

$$P_a = \left(0.25 f_m' A_n + 0.65 A_{st} F_s\right)\left[1 - \left(\frac{h}{140r}\right)^2\right] \quad (1)$$

where f'_m is the compressive strength of the masonry prism, A_n is the net cross-sectional area, A_{st} is the area of reinforcing bar, F_s is the allowable compressive stress of the reinforcing bar as shown in Table 2, and h/r is the slenderness ratio. The value of f'_m was determined from the prism test without multiplying with the height-to-thickness correction factor and A_n was the load bearing area. It should be noted, Eqn. (1) was developed by using the factor of safety of 4.0 and 3.85 against the failure of the masonry prism and the reinforcing bar, respectively.

From Table 5, the ratios of the observed ultimate load to the allowable load are in the range of 2.07 and 3.66 with an average of 2.72 and a coefficient of variation (COV) of 0.19. Performing the normality test, the distribution of the ratios had the correlation (R-value) of 0.9374, which can be assumed as normal distribution. In practice, the probability of failure of the masonry walls (the probability that the masonry walls have the ratios of the ultimate load to the allowable load less than 1.0) is usually set to be at least 1/10000 [15], corresponding to a reliability of 99.99% and a reliability index of 3.72. By analyzing the data, the probability of failure of the wall specimens was found to be 1/2460, which is over 4 times greater than the recommended value. In addition, the mean value of the ratios is quite low compared to the factor of safety of 3.0 to 4.0 which is used in deriving the allowable stress design equation for the masonry wall under axial load. Therefore, Eqn. (1) should be modified for the mortarless reinforced concrete masonry wall.

Table 5 Observed ultimate load, ACI and proposed allowable axial loads, and their ratios

Specimen number	P_{ult} (kN)	P_a (kN)	P'_a (kN)	P_{ult}/P_a	P_{ult}/P'_a
C-076-1P	237.7	65.00	56.13	3.66	5.95
C-247-1P	189.3	55.29	47.75	3.42	5.57
C-285-1P	178.0	51.78	44.71	3.44	5.60
C-076-2F	222.9	88.24	74.86	2.53	3.70
C-247-2F	185.6	72.74	61.71	2.55	3.74
C-285-2F	174.4	67.07	56.90	2.60	3.81
C3-076-P	233.7	86.83	77.96	2.69	5.85
C3-247-P	194.6	73.87	66.32	2.63	5.73
C3-285-P	180.7	69.17	62.11	2.61	5.68
C4-076-F	224.1	108.08	94.70	2.07	3.72
C4-247-F	195.4	89.10	78.07	2.19	3.94
C4-285-F	185.4	82.16	71.98	2.26	4.05

Apart from the mortarless, there are a number of unavoidable factors that reduce the axial ultimate load of the masonry walls such as load eccentricity, member misalignment, and member's out-of-straightness. These factors are associated with the slenderness ratios of the walls and their ultimate load reduction effects were included in the slenderness-reduction factor. To examine this effect, the dimensionless ratio of the wall strength to the compressive strength of the masonry was plotted against the slenderness ratio as shown in Fig. 12. The compressive strength of the masonry was taken as the averaged nominal bearing strength of the specimens with 0.760 m high. It was found that the calculated ratios compare well with the curve of the ACI strength-reduction factor. Therefore, it can be assumed that the slenderness-reduction factor of the mortarless masonry walls has the form of the ACI slenderness-reduction factor.

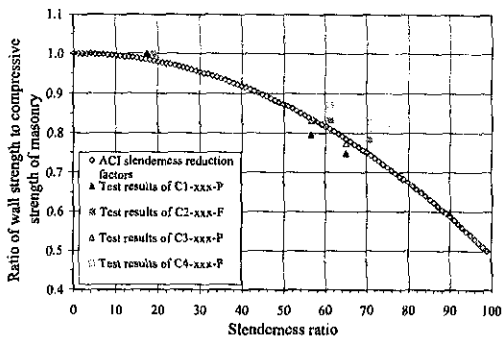

Fig. 12 Ratio of wall strength to compressive strength of masonry and slenderness ratio

From Table 5, it can be seen that increasing the reinforcement ratio and grouting area decreased the ratios of the ultimate axial load to the allowable axial load considerably. This is due to the fact that Eqn. (1) includes both factors in the prediction of the allowable axial load. From the test results, however, neither factors influenced the bearing load capacity of the wall specimens. This is as expected since the reinforcing bars yielded at the strain of 0.0012, long before the ultimate strain of 0.002 to 0.003 of the masonry was reached. In addition, all specimens had the same load bearing area and failed in the same crushing and tearing mode. Therefore, it was concluded that the contribution of reinforcing bars to the bearing strength of the mortarless masonry wall is small and should be neglected. The bearing strengths were found to be 8.45 and 11.32 MPa for specimen group 1 and 3 (partially grouted specimens) and 8.30 and 10.67 MPa for specimen group 2 and 4 (fully grouted specimens). These values were typically lower than the compressive strength of the mortarless masonry prisms as shown in Table 1. This indicates that there is no confinement of the bearing area by surrounding grout and masonry and that there is stress concentration under the bearing area. Therefore, the design rules for the concentrated load distribution specified in ACI 530-99 should not be applied for the mortarless masonry in this case. However, as shown in [12], the bearing strength can be increased by using bond beam and/or larger bearing plate. This problem requires further investigation.

There are a number of factors that contribute to the variations in the compressive strength of the masonry prisms such as the variation in the dimensions, in the material properties, and in the construction practices. In this study, the variation in the dimensions was considered to be the major factor that gives a higher variation of the compressive strength of the mortarless masonry prisms compared to the variation of the mortar jointed prism. Based on the statistical analysis of the data obtained in [16], the COV of the mortar jointed prism was found to be 0.15 and since there is a limit number of test data in this study, the COV of the compressive strength of the mortarless prisms was assumed to be 0.20, which is 33% larger than that of the mortar jointed prism. Therefore, the factor of safety associated with the compressive strength of the masonry prism should be increased from 4.0 to 4.44, which is similar to that used in the EIT 1005-75. Therefore, the proposed design equation should be in the form of

$$P_a' = 0.225 f_m' A_n \left[1 - \left(\frac{h}{140r} \right)^2 \right] \tag{2}$$

From Table 5, Eqn. (2) gives the ratio of the ultimate load to the allowable load between 3.70 and 5.95 with an average of 4.78 and a COV of 0.21, which is larger than the recommended

factor of safety of 3.0 to 4.0. Performing the normality test, it was found that the distribution of the ratios can be assumed as a normal distribution with R-value of 0.8891. Thus, the probability that the ratio is less than 1.0 is about 1/12000 with the reliability index of 3.77.

4.4 Comparisons of the transverse load test results with the design equations

Table 6 shows the experimental flexural strength, M_{exp}, the allowable moment, M_a, the proposed allowable moment, M_a', and the ratios of the tested flexural strength to the allowable moment. The allowable moment was calculated from the flexural equations in [13]. It was taken from the smaller of the moment controlled by the allowable flexural compressive strength of the masonry, M_m, and the moment controlled by the allowable tensile strength of the steel reinforcing bar, M_t, where

$$M_m = \frac{b_e d^2 kj F_b}{2} \tag{3}$$

$$M_t = A_s jd F_s \tag{4}$$

where b_e is the effective width for a reinforcing bar and is taken as the center-to-center distance of the reinforcing bars, d is the distance from the compressive surface of the masonry wall to the reinforcing bar, k can be calculated from $k = \sqrt{(n\rho)^2 + 2n\rho} - n\rho$, where n is the modular ratio which is the ratio of the modulus of elasticity of the steel and masonry and ρ is steel reinforcement ratio, j can be calculated from $j = 1 - (k/3)$, F_b is the allowable flexural compressive strength of the masonry, equal to $(1/3)f_m'$, and F_s is the allowable tensile stress of the reinforcing bar. It should be noted that the factor of safety of 3.33 of F_b in Eqn. (3) is determined from the test data in which the compressive stress at failure for hollow masonry subjected to flexure is larger than that for the masonry under axial load by 33% [18]. The factors of safety of F_s are 2.0 for steel grade 40 and 50 and 2.5 for steel grade 60.

Table 6 shows that the ratio of the tested flexural strength to the allowable moment ranges between 1.84 and 2.93 with an average of 2.32 and a COV of 0.17. Performing the normality test, the distribution of the ratios can be assumed to be a normal distribution with R-value of 0.9468. The probability of failure of the ratios is 1/1950, which is more than 5 times larger than the recommended value. In addition, the mean value of the ratio is quite low compared to the factor of safety of 2.5 to 3.0 generally used in the development of the allowable stress design equation for masonry wall under flexure [13]. Therefore, the equations for mortarless reinforced concrete masonry wall should be modified.

Due to the lack of the test data to confirm the increasing in the flexural compressive strength of the mortarless masonry compared to the axial compressive strength and to account for the quality of the masonry units, the factor of safety for F_b in Eqn. (3) should be the same as that for f_m' for axial compression. Using this allowable flexural compressive strength, it can be seen that the ratio of the flexural strength to the allowable moment is in the range of 2.36 and 3.82 with an average of 2.82 and a COV of 0.17. This is in good agreement with the recommended factor of safety. Performing the normality test, it was found that the

distribution of the ratios fits normal distribution with R-value of 0.9252. The probability that the ratio is less than 1.0 is 1/14700 with the reliability index of 3.82.

Table 6 Experimental flexural strength, ACI and proposed allowable moments, and their ratios

Specimen number	M_{exp} (kN-m)	M_a (kN-m)	M'_a (kN-m)	M_{exp}/M_a	M_{exp}/M'_a
F1-237-P	9.17	4.16	3.708	2.21	2.47
F1-275-P	8.75	4.16	3.708	2.10	2.36
F2-237-F	13.88	4.74	4.741	2.93	2.93
F2-275-F	11.62	4.74	4.741	2.45	2.45
F3-237-P	13.73	6.54	4.428	2.10	3.10
F3-275-P	12.04	6.54	4.428	1.84	2.72
F4-237-F	23.63	8.17	6.187	2.89	3.82
F4-275-F	16.64	8.17	6.187	2.04	2.69

5. CONCLUSIONS

From the study, the following conclusions can be drawn.

1. The mortarless masonry wall specimens under concentric axial load showed large initial deformation soon after loading to about 35% of the compressive strength due to the uneven surfaces of the units. Two types of cracks were also observed during this initial loading: cracks due to load transfer caused by unequal friction that obstructs lateral deformation of the masonry units and cracks due to flexural movements caused by height tolerances of the masonry units in a course. They are occurred until full contact between the masonry units was reached. However, this initial deformation is quite small for the specimens under transverse loads.

2. The relationship of concentric axial load and axial deformation was linear up to 65-80% of the ultimate axial load. Failure was due to tearing and crushing of the masonry in the region beneath the bearing plate with shear line in the diagonal direction extending from that region along the specimen height. The shear line angle was 20 to 30 degree to the vertical for fully grouted walls and 25 to 35 degree to the vertical for partially grouted walls. Therefore, the design rules for concentrated load dispersion specified in ACI 530-99 should not be applied for the mortarless masonry in this case. Due to this failure mode, increasing the steel reinforcing area and grouting area do not increase the ultimate bearing strength of the walls.

3. The relationship of transverse load to mid-span deflection is bilinear with a larger stiffness in the first linear segment. At the end of the first linear segment, large deflection at mid-span of the wall with the yielding of steel reinforcement was observed. Failure was due to crushing of the masonry units on the compression surface with large tensile cracks on the tension zone. Increasing the steel reinforcing area and grouting area increase the flexural strength, which is in according with the results from the design equations.

4. For concentrated axial load, the design equation should be in the form of Eqn. (2). This equation gives a ratio of the ultimate load to the allowable load in the range of 3.70 and 5.95 with an average of 4.78 and a COV of 0.21. For transverse load, the Eqn. (3) with the flexural allowable compressive strength of $F_b = 0.225 f'_m$ and Eqn. (4) should be used. These

equations give the ratio of the flexural strength to the allowable moment in the range of 2.36 and 3.82 with an average of 2.82 and a COV of 0.17.

REFERENCES

1. Marzahn, G., "Investigation on the Initial Settlement of Dry-Stacked Masonry under Compression", In. LACER No. 4, Universität Leipzig, 1999.
2. Marzahn, G., "A Study on the Creep Behavior of Dry-Stacked Masonry Walls and Individual Masonry Units", In. LACER No. 5, Universität Leipzig, 2000.
3. Marzahn, G., "Dry-Stacked Masonry in Comparison with Mortar Jointed Masonry", In. LACER No. 2, Universität Leipzig, 1997.
4. Building Code Requirements for Masonry Structures (ACI 530-99/ASCE 5-99/TMS 402-99), Masonry Jointed Committee, ACI/ASCE/TMS. CO., 1999.
5. Standard Specification for Loadbearing Concrete Masonry Units. (2000). C90-00. ASTM. PA.
6. Standard Specification for Grout for Masonry. (1999). C476-99. ASTM. PA.
7. Standard Test Methods for Sampling and Testing Concrete Masonry Units and Related Units. (1999). C140-99b. ASTM. PA.
8. Standard Test Method for Sampling and Testing Grout. (2000). C1019-00b. ASTM. PA.
9. Test Methods for Compressive Strength of Laboratory Constructed Masonry Prisms. (1997). E447-97. ASTM. PA.
10. Standard Test Methods for Tension Testing of Metallic Materials. (2000). E8-00b. ASTM. PA.
11. Standard Specification for Mortar for Unit Masonry. (2000). C270-00. ASTM. PA.
12. Page, A.W. and Shrive, N.G., "Concentrated Loads on Hollow Concrete Masonry", *ACI Structural Journal*, 1990, Vol. 87. No. 4. pp. 436-444.
13. Matthys, J.H., "Masonry Designer's Guide", The Masonry Society. CO. USA, 1993.
14. Standard Test Method for Flexural Strength of Concrete (Using Simple Beam with Third-Point Loading). (2000). C78-00. ASTM. PA.
15. Harr, M.E., "Reliability-Based Design in Civil Engineering", 1st Ed. McGraw-Hill, New York, 1987.
16. Seangatith, S. and Chaijaruwanich, J., "Compressive Strength of Concrete Masonry Units and Prisms", *Suranaree Journal of Science and Technology*, 2001, Vol. 8. No 3. pp. 131-137.
17. Standard for Masonry Structures (EIT 1005-75). (1975). Engineering Institute of Thailand. Bangkok.
18. Commentary on Building Code Requirements for Masonry Structure (ACI 530-99/ASCE 5-99/TMS 402-99). (1999). Masonry Jointed Committee. ACI/ASCE/TMS. CO.

ACKNOWLEDGEMENTS

The research work presented in this paper has been sponsored by Suranaree University of Technology under the project number SUT7-712-47-12-05; this support is gratefully acknowledged. The author also would like to thank Assoc. Prof. Dr. Amnat Apichatvullop for his suggestions. The results presented herein represent the views and opinions of the writer only.